Electronic Supporting Information (ESI)

Electron density effect of aromatic carboxylic acids in naphthalenediimide-based coordination polymers: from thermal electron transfer and charge transfer to photoinduced electron transfer

Gao-Peng Li,[a,*] Jing Zhang[a], Wan-Wan Ren[a], Si-Nan Wang[a], Ying-Xia Wang[a], Yun-Long Fu[a,*] and Yao-Yu Wang[b,*]

[a]*Key Laboratory of Magnetic Molecules and Magnetic Information Materials of the Ministry of Education, School of Chemistry and Material Science, Shanxi Normal University, Taiyuan 030031, China*

[b]*Key Laboratory of Synthetic and Natural Functional Molecule Chemistry of the Ministry of Education, Shaanxi Key Laboratory of Physico-Inorganic Chemistry, College of Chemistry and Materials Science, Northwest University, Xi'an, Shaanxi 710127, P. R. China*

Corresponding Authors

E-mail: nwuligp@163.com, yunlongfu@sxnu.edu.cn, wyaoyu@nwu.edu.cn

Table of Content

Section S1. General information. 3
S1-1. Materials and General Methods. 3
S1-2. Synthetic Methods....4
S1-3. X-ray Crystallographic Measurements. 4
S1-4. Computational Methods. 5
Section S2. Figures and Tables 6
Table S1. Crystal Data and Structure Refinement for 1 and 2. 6
Table S2. Selected bond lengths [Å] for 1 and 2. 7
Table S3. Selected bond angles [°] for 1 and 2. 8
Fig. S1 The asymmetric unit of 1 (a) and 2 (b). 9
Fig. S2 The coordination environment of Cd^{2+} ion in 1 (a) or 2 (b). Cd: light cyan; C: grey; O: red; N: blue; H: yellow. 10
Fig. S3 The π···π, lone pair···π and hydrogen bonds interactions of layers in 1 (a) and 2 (b). 11
Fig. S4 PXRD patterns of 1 (a) and 2 (b) simulated from the X-ray single-crystal structures, as-synthesized samples and after irradiation samples. 12
Fig. S5 TGA plots of 1 (a) and 2 (b). 13
Fig. S6 Solid-state UV-vis absorption spectra of 1 and 2. 14
Fig. S7 The optical band gaps of 1 and 2 based on UV-vis absorption spectra using the Kubelka-Munk function. 14
Fig. S8 FT-IR spectra of 1 (a) and 2 (b). 15
Fig. S9 O 1s (a and b) C 1s (c and d) and Cd 3d (e and f) XPS core-level spectra of 1 (top) and 2 (bottom). 16
Fig. S10 The crystal orbitals of 1. 17
Fig. S11 The crystal orbitals of 2. 17
Section S3. References 18

Section S1. General information.

S1-1. Materials and General Methods.

All chemicals are commercially available and were used without further purification. Powder X-ray diffraction (PXRD) data were collected on a Rigaku UItima IV-185 diffractometer with a scan rate of 5°/min in the range of 5-50° at room temperature. An infrared (IR) spectrum was obtained through a Nicolet 5DX spectrometer together with a KBr pellet from 4000 to 400 cm^{-1}. A 300 W mercury (Hg) lamp (365 nm) system with temperature control equipped with an IR filter was used to prepare colored samples for UV-vis spectrophotometer studies, and the distances between these samples and the Hg lamp were around 20 cm. The solid-state UV-vis absorption spectra were obtained at room temperature in the reflectance diffuse mode on a METASH UV-9000S UV-vis spectrophotometer, and a $BaSO_4$-coated glass slide as a reference. Thermogravimetric analyses (TGA) were carried out in a N_2 stream using STA-449-F5 thermogravimetric analyzer at a heating rate of 10 °C min^{-1}. Electron paramagnetic resonance (EPR) spectra were recorded on a Bruker A300-10/12 electron paramagnetic resonance spectrometer with a 100 kHz magnetic field in the X-band at ambient temperature.

S1-2. Synthetic Methods

Syntheses of $[Cd_2(H_2NDI)(IPA)_2(H_2O)_2]$ (1)

A mixture of $Cd(NO_3)_2·4H_2O$ (0.0308 g, 0.1 mmol), H_2NDI(0.0227 g, 0.05 mmol), IPA (0.0166 g, 0.1 mmol), and H_2O/DMF (4 mL/1 mL) was ultrasonically treated for 5 min and then transferred to a 15 mL Teflon-lined, heated to 120°C, and maintained at this temperature for 48 h. Yellow crystals were obtained, which were then collected and washed with DMF and sealed for preservation in the dark. Yield: 30.2%. Elem. Anal. Calcd for $C_{20}H_{15}CdN_3O_7$: C, 46.00; H, 2.87; N, 8.05. Found: C, 45.87; H, 2.45; N, 8.65. IR (KBr, cm-1): 3513(m), 3438(m), 3139(w), 2922(w), 1713(s), 1658(s), 1602(s), 1541(s), 1452(m), 1391(s), 1347(s), 1245(s), 1211(w), 1061(w), 990(w), 838(m), 790(m), 736(m), 654(w).

Syntheses of $[Cd_2(H_2NDI)(IPA\text{-}OH)_2(H_2O)_2]$ (2)

Compound 2 was prepared following the procedure for **1**, except that 0.0182 mg of H_2IPA-OH was used instead of H_2IPA. Yield: 32.7%. Elem. Anal. Calcd for $C_{20}H_{15}CdN_3O_8$: C, 44.63; H, 2.79; N, 7.81. Found: C, 44.47; H, 2.45; N, 8.35. IR (KBr, cm-1): 3594 (m), 3482(m), 3146(w) 1713(s), 1666(s), 1544(s), 1475(w), 1448(w), 1361(s), 1255(s), 1171(s), 1068(w), 1955(w), 987(w), 966(w), 865(w), 831(m), 770(s), 729(m), 586(w).

S1-3. X-ray Crystallographic Measurements.

Single-crystal X-ray diffraction (SCXRD) measurements were carried out on a Bruker Apex II CCD diffractometer with graphite-monochromated Mo-Kα radiation (λ = 0.71073 Å) at 298 K. The structures were solved using the direct method (SHELXS) and refined by means of the full matrix least-squares method (SHELXL) on F^2.[1] Anisotropic thermal parameters were used for the non-hydrogen atoms and isotropic parameters for the hydrogen atoms. Hydrogen atoms were added geometrically and refined using a riding model.

S1-4. Computational Methods.

Density functional theory (DFT) calculations for the periodic unit cell of **1** and **2** were carried out using CASTEP program.[2] The generalized gradient approximation (GGA) as formulated by the Perdew-Burke-Ernzerhof (PBE) functional was used as the exchange-correlation potential. The effect of the van der Waals (vdW) interaction is taken into account using the semiempirical dispersion correction of the Tkatchenko-Scheffler (TS) scheme (PBE-D(TS)). The ultra-soft pseudopotential (uspp) was used as the plane wave basis set to describe the electron-ion interactions. The cutoff energy of the plane wave basis is 340 eV. The conjugate gradient method is employed for geometry optimization using a 2 × 2 × 1 Monk-horst-Pack k-point mesh size. The energy, maximum force and maximum stress tolerances of geometry optimization are set to 1×10^{-5} eV $atom^{-1}$, 0.03 eV $Å^{-1}$ and 0.05 GPa, respectively. The electronic structures of **1** and **2**, including the band structure and the density of states (DOS) were calculated at the same level as the geometry optimization, since more precise calculations for such a large system (92 atoms per unit cell for **1** and 94 atoms per unit cell for **2**) are extremely time consuming. Nevertheless, the GGA obtained electronic structures are commonly reasonable, especially for describing the electronic arrangement which is the main focus in this work.

For the anionic (IPA and IPA-OH) and neutral H_2NDI ligands, DFT calculations were performed using Gaussian 09 program.[3] The geometries of these molecules were optimized at B3LYP/6-31G(d, p) level. Frequency calculations, at the same level of theory, were used to obtain stable structure.

Section S2. Figures and Tables

Table S1. Crystal Data and Structure Refinement for 1 and 2.

Compound	1	2
Formula	$C_{20}H_{15}CdN_3O_7$	$C_{20}H_{15}CdN_3O_8$
Formula weight	521.75	537.75
Crystal system	Ticlinic	Ticlinic
Space group	*P*-1	*P*-1
a (Å)	9.6549(7)	9.7966(6)
b (Å)	10.4770(8)	10.2903(7)
c (Å)	10.7029(8)	10.4954(7)
α (deg)	98.353(2)	96.946(2)
β (deg)	113.1100(10)	96.6190(10)
γ (deg)	96.380(2)	111.5650(10)
V (Å^3)	968.24(13)	962.03(11)
Z	2	2
ρ_{cal} (g cm^{-3})	1.790	1.856
μ (mm^{-1})	1.179	1.193
F(000)	520.0	536.0
Reflections collected	9942	17204
R_{int}	0.0302	0.0214
Data/restraints/parameters	3762/1/285	4732/8/298
GOF on F^2	1.048	1.151
R_1[a] [I > 2σ(*I*)]	0.0219/0.0576	0.0236/0.0593
wR_2 (all data)	0.0230/0.0581	0.0257/0.0601

$R_1 = \sum||F_O| - |F_C||/\sum|F_O|$ $wR_2 = [\sum w(|F_O|^2 - |F_C|^2)^2 / \sum w(F_O^2)^2]^{1/2}$

Table S2. Selected bond lengths [Å] for **1** and **2**.

1		**2**	
Cd1-O3	2.2953(15)	Cd1-O6[1]	2.4570(16)
Cd1-O6[1]	2.5032(16)	Cd1-O5[1]	2.3156(14)
Cd1-O6[2]	2.3101(16)	Cd1-O4[2]	2.5106(16)
Cd1-O5[2]	2.4640(16)	Cd1- O4	2.2709(15)
Cd1- O4	2.5051(18)	Cd1-O1W	2.3215(18)
Cd1-O1W	2.3266(17)	Cd1-O3	2.5538(17)
Cd1-N1	2.2639(17)	Cd1-N1	2.2557(17)

Symmetry codes for **1**: #1 1-x, 1-y, -z; #2 -1+x, y, z; #3 1+x, y, z; #4 1-x, 2-y, 2-z; Symmetry codes for **2**: #1 1+x, y, z; #2 1-x, -y, 1-z; #3 -1+x, y z; #4 2-x, 2-y 2-z.

Table S3. Selected bond angles [°] for **1** and **2**.

1		**2**	
O3- Cd1- O6^{1}	126.16(6)	O6^{1}- Cd1- O4^{2}	81.98(5)
O3- Cd1- O6^{2}	83.30(6)	O6^{1}- Cd1- O3	116.63(6)
O3- Cd1- O5^{1}	156.95(7)	O5^{1}- Cd1- O6^{1}	54.91(5)
O3- Cd1- O4	54.29(5)	O5^{1}- Cd1- O4^{2}	85.21(5)
O3- Cd1- O1W	80.33(6)	O5^{1}- Cd1- O1W	81.44(6)
O6^{1}- Cd1- O6^{2}	72.34(6)	O5^{1}- Cd1- O3	159.37(6)
O6^{1}- Cd1- O5^{1}	54.36(5)	O4- Cd1- O6^{1}	78.07(5)
O6^{1}- Cd1- O4	75.20(5)	O4- Cd1- O5^{1}	130.58(5)
O6^{2}- Cd1- O4	82.99(6)	O4- Cd1- O4^{2}	72.97(6)
O6^{1}- Cd1- O1W	120.43(6)	O4- Cd1- O1W	116.20(6)
O5^{1}- Cd1- O6^{2}	115.23(5)	O4- Cd1- O3	53.41(5)
O5^{1}- Cd1- O4	111.90(6)	O4^{2}- Cd1- O3	113.42(5)
O1W- Cd1- O6^{2}	163.33(6)	O1W- Cd1- O6^{1}	90.37(7)
O1W- Cd1- O5^{1}	81.40(6)	O1W- Cd1- O4^{2}	166.65(5)
O1W- Cd1- O4	89.94(7)	O1W- Cd1- O3	79.78(6)
N1- Cd1- O3	107.06(6)	N1- Cd1- O6^{1}	153.50(7)
N1- Cd1- O6^{1}	114.68(6)	N1- Cd1- O5^{1}	104.59(6)
N1- Cd1- O6^{2}	80.22(6)	N1- Cd1- O4	113.75(6)
N1- Cd1- O5^{1}	90.30(7)	N1- Cd1- O4^{2}	79.43(6)
N1- Cd1- O4	156.42(7)	N1- Cd1- O1W	103.90(7)
N1- Cd1- O1W	101.62(7)	N1- Cd1- O3	88.21(7)

Symmetry codes for **1**: #1 1-x, 1-y, -z; #2 -1+x, y, z; #3 1+x, y, z; #4 1-x, 2-y, 2-z; Symmetry codes for **2**: #1 1+x, y, z; #2 1-x, -y, 1-z; #3 -1+x, y z; #4 2-x, 2-y 2-z.

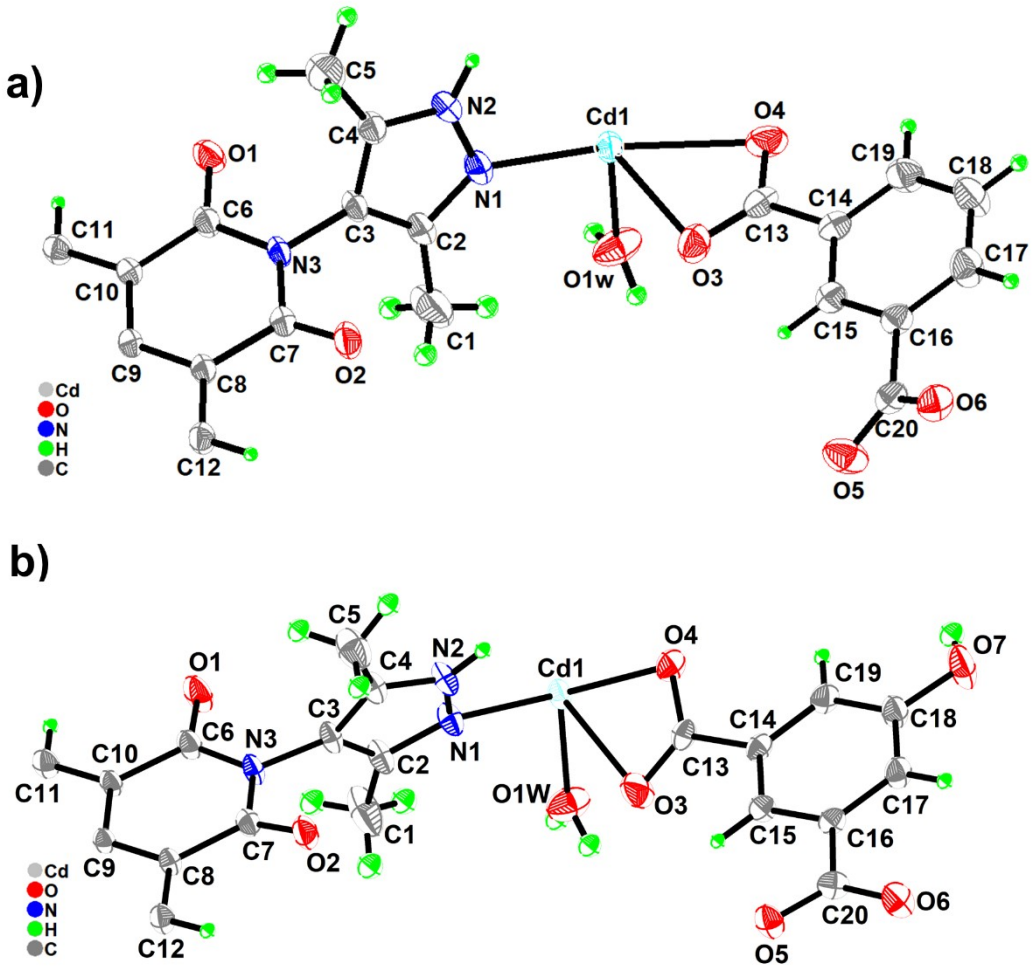

Fig. S1 The asymmetric unit of 1 (a) and 2 (b).

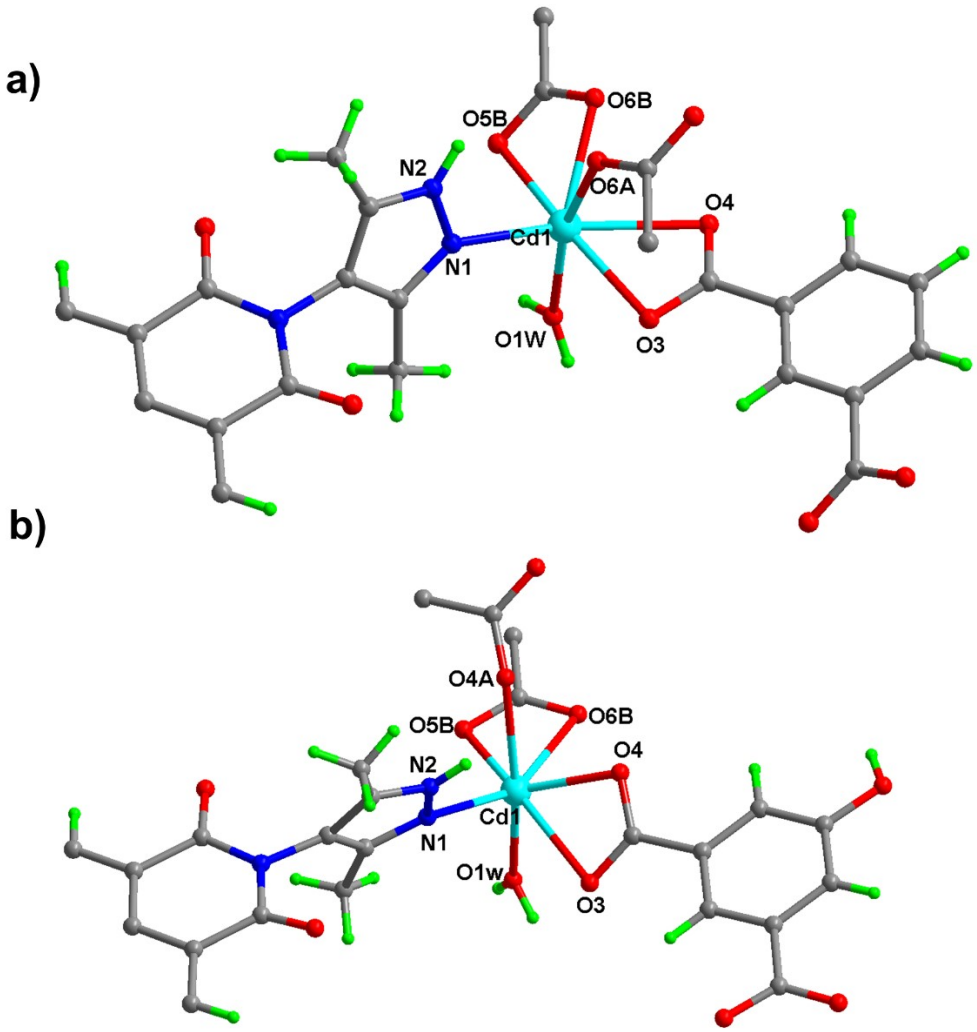

Fig. S2 The coordination environment of Cd^{2+} ion in 1 (a) or 2 (b). Cd: light cyan; C: grey; O: red; N: blue; H: yellow.

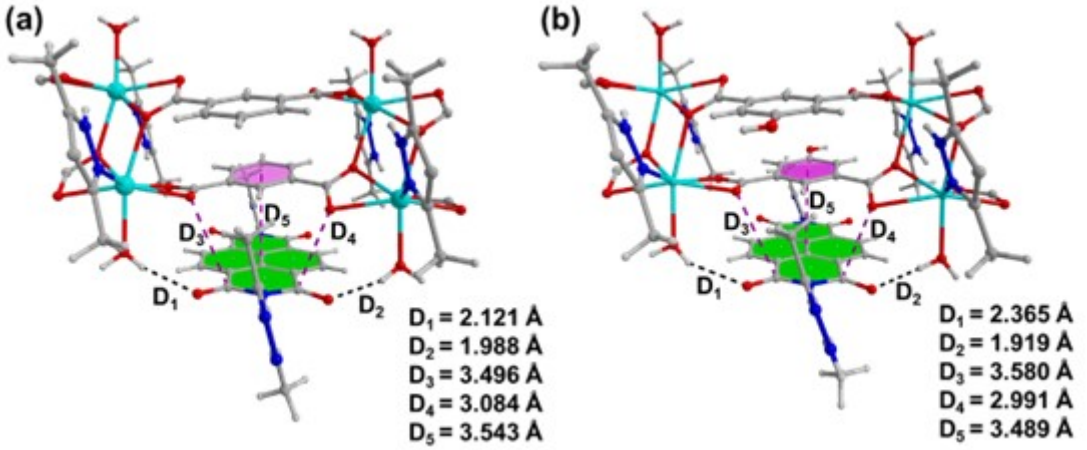

Fig. S3 The π···π, lone pair···π and hydrogen bonds **interactions of layers** in **1** (a) and **2** (b).

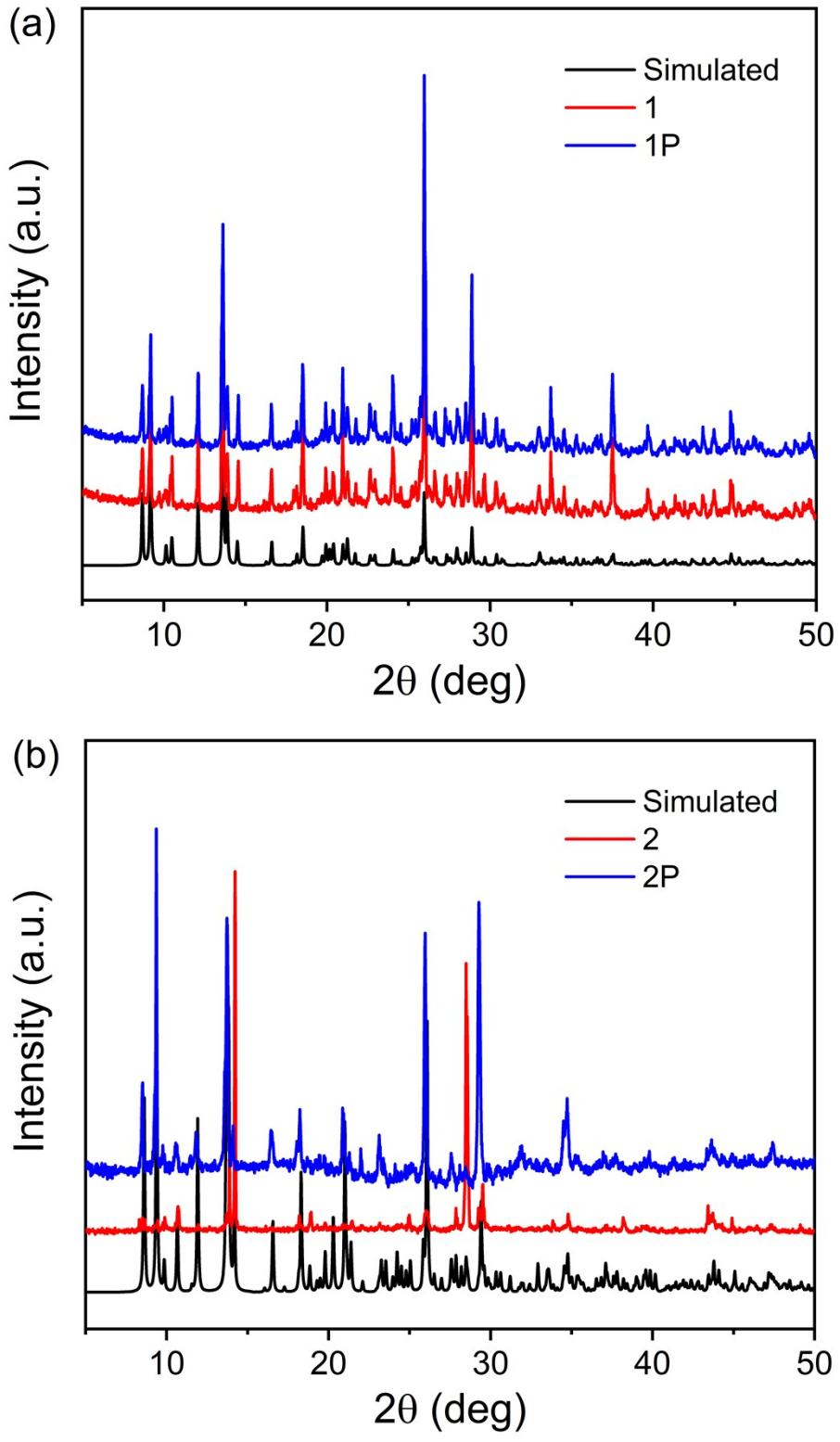

Fig. S4 PXRD patterns of **1** (a) and **2** (b) simulated from the X-ray single-crystal structures, as-synthesized samples and after irradiation samples.

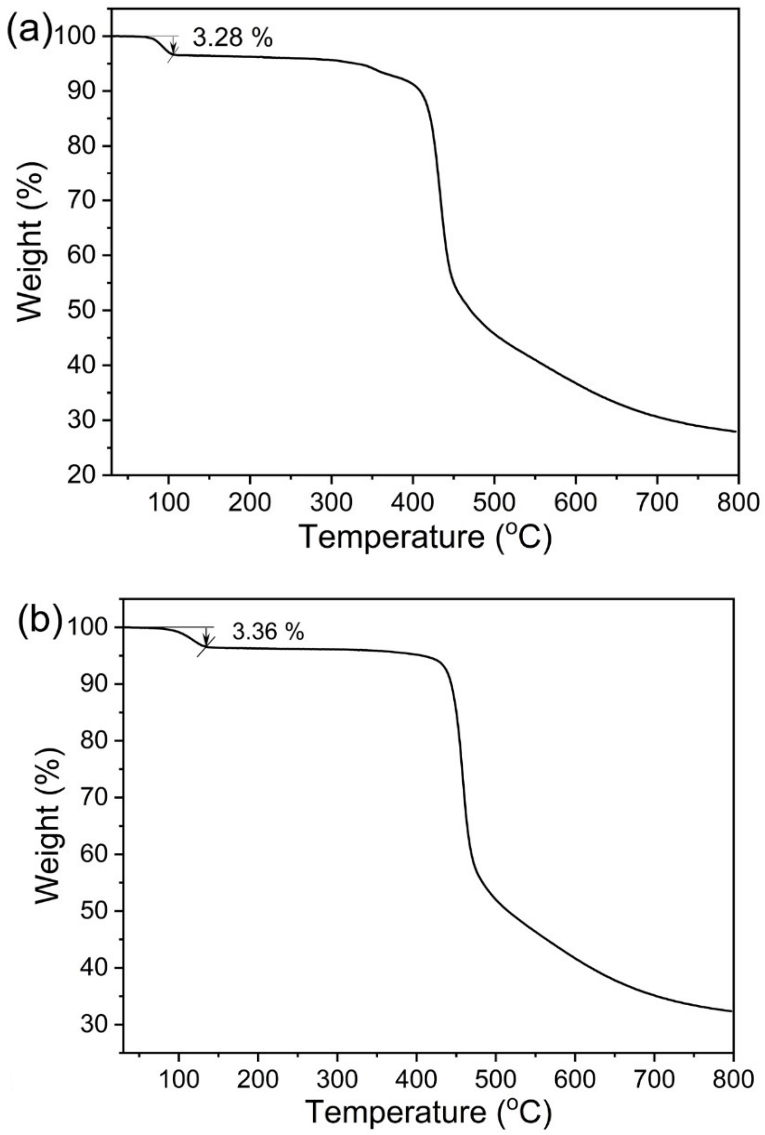

Fig. S5 TGA plots of **1** (a) and **2** (b).

Details: **1** releases all water molecules before 410.5 °C with a total weight loss of 3.28% (Calcd 3.45%), and the framework begins to collapse as the temperature continues to rise. **2** indicates 3.36 % weight loss (calcd 3.35%) below 134.5 °C, which corresponds to the release of all coordinated H_2O molecules. Also, no obvious weight loss occurs before the main structure collapses at 435.3 °C. The thermal stabilities for these two compounds are significantly higher than those of most reported MOFs. In general, the TGA results for these two compounds are in consistent with their structural and elemental analyses.

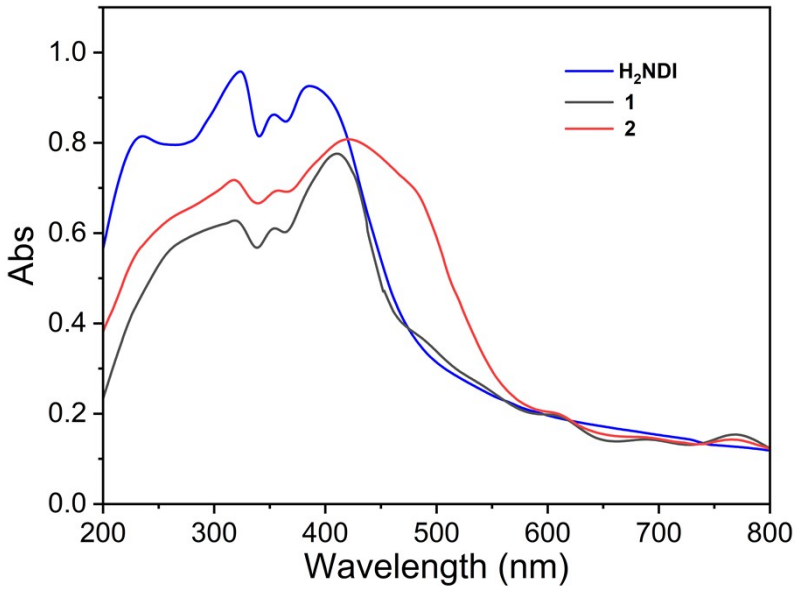

Fig. S6 Solid-state UV-vis absorption spectra of **1** and **2**.

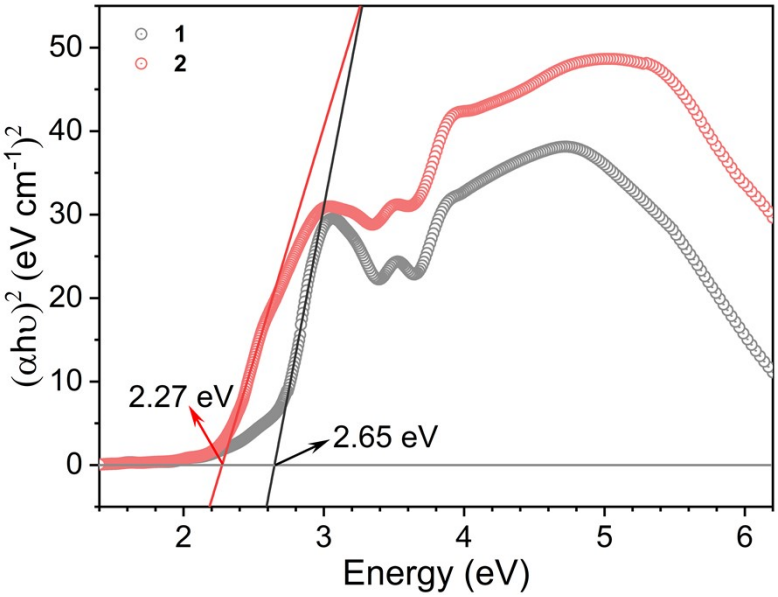

Fig. S7 The optical band gaps of **1** and **2** based on UV-vis absorption spectra using the Kubelka-Munk function.

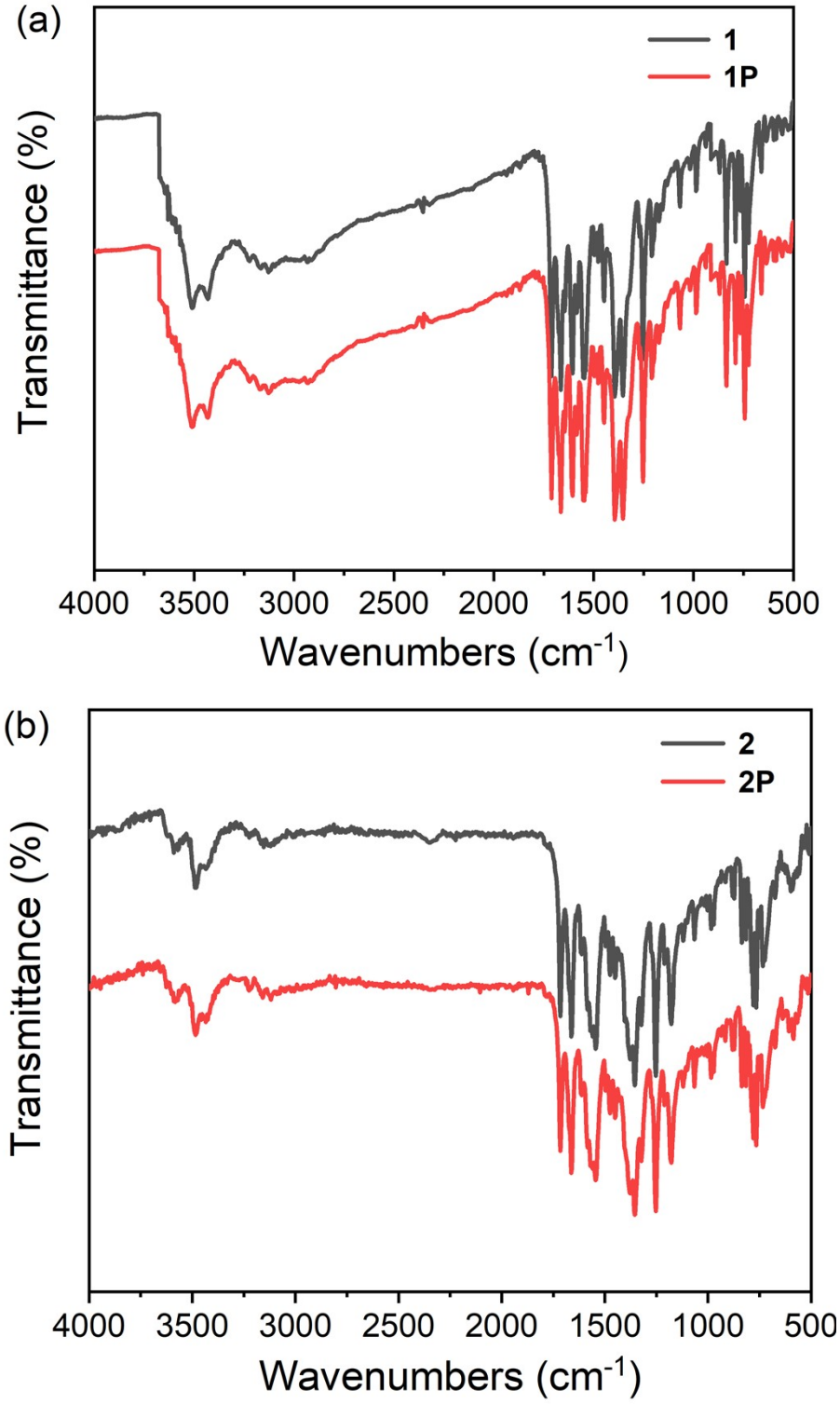

Fig. S8 FT-IR spectra of **1** (a) and **2** (b).

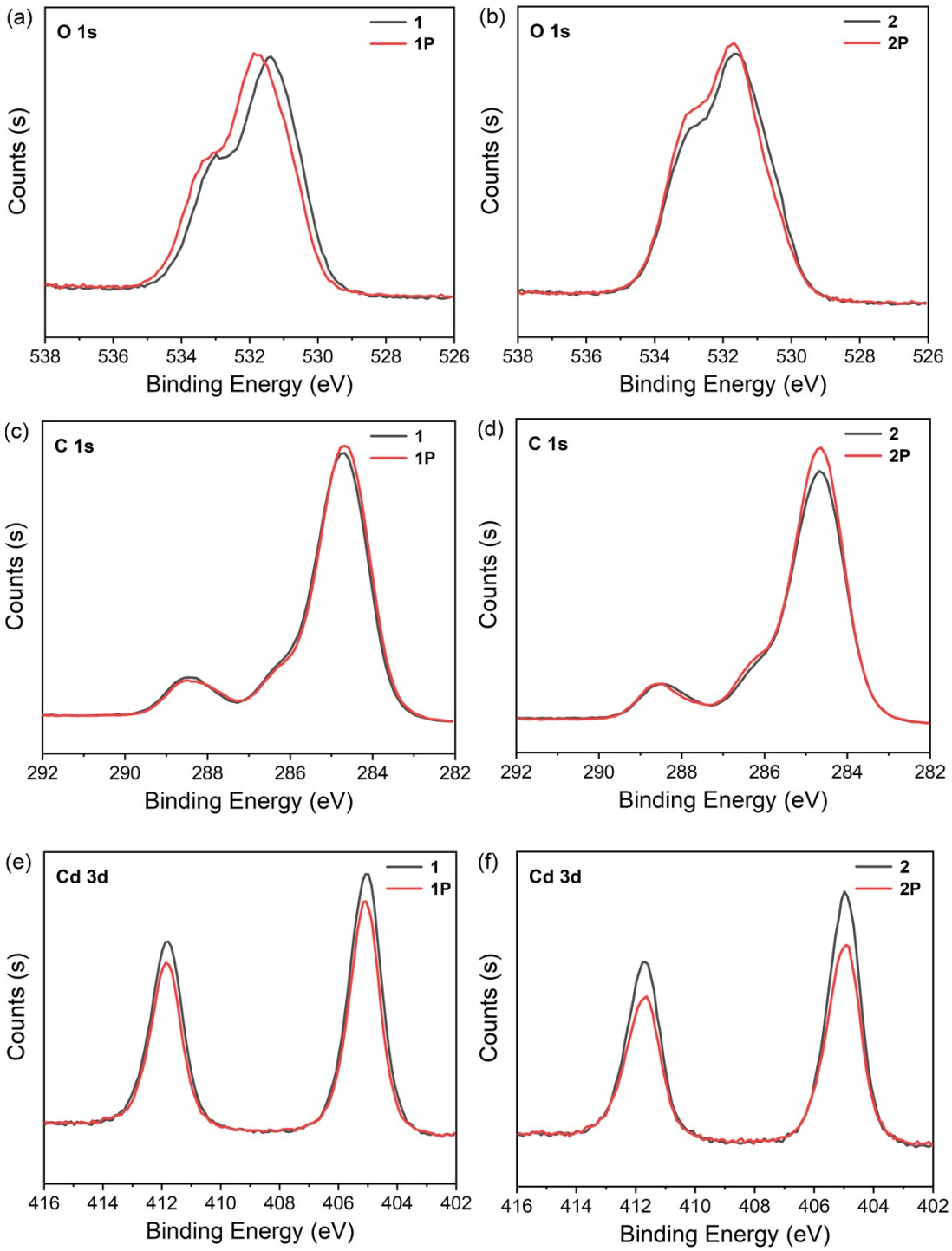

Fig. S9 O 1s (a and b) C 1s (c and d) and Cd 3d (e and f) XPS core-level spectra of **1** (top) and **2** (bottom).

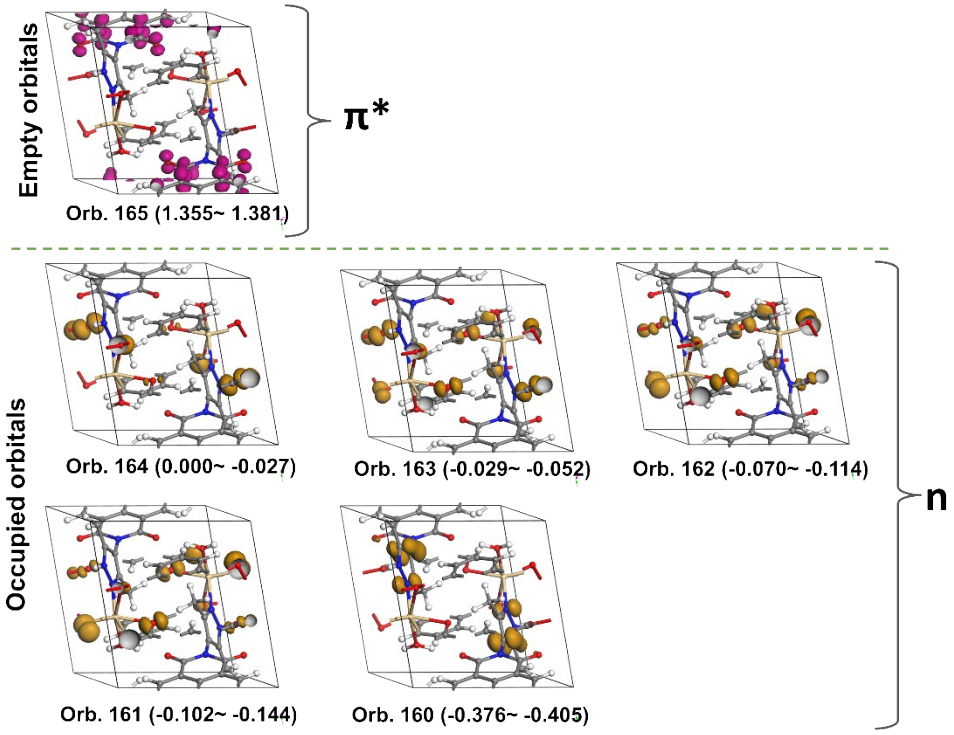

Fig. S10 The crystal orbitals of **1**.

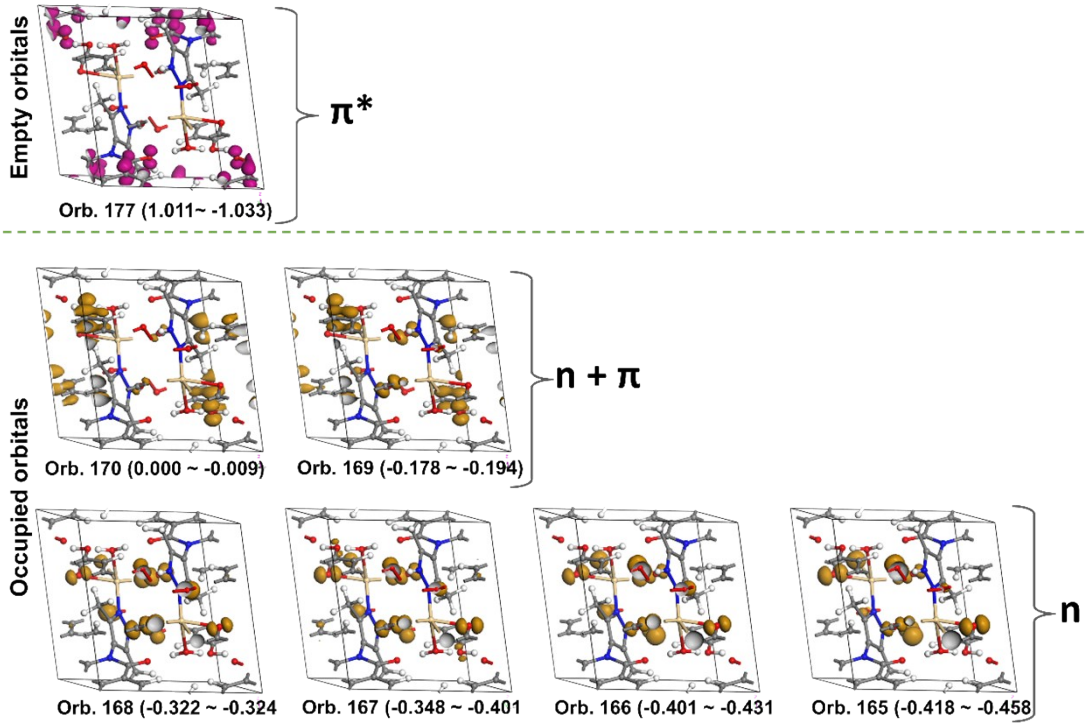

Fig. S11 The crystal orbitals of **2**.

Section S3. References

1. G. M. Sheldrick, *Acta Crystallogr. Sect. A: Found. Crystallogr.*, 2008, **64**, 112-122.
2. S. J. Clark, M. D. Segall, C. J. Pickard, P. J. Hasnip, M. I. Probert, K. Refson and M. C. Payne, *Z. Krist-Cryst. Mater.*, 2005, **220**, 567-570.
3. R. E. Gaussian 09, Frisch, M. J.; Trucks, G. W.; Schlegel, H. B.; Scuseria, G. E.; Robb, M. A.; Cheeseman, J. R.; Scalmani, G.; Barone, V.; Mennucci, B.; Petersson, G. A.; Nakatsuji, H.; Caricato, M.; Li, X.; Hratchian, H. P.; Izmaylov, A. F.; Bloino, J.; Zheng, G.; Sonnenberg, J. L.; Hada, M.; Ehara, M.; Toyota, K.; Fukuda, R.; Hasegawa, J.; Ishida, M.; Nakajima, T.; Honda, Y.; Kitao, O.; Nakai, H.; Vreven, T.; Montgomery, J. A., Jr.; Peralta, J. E.; Ogliaro, F.; Bearpark, M.; Heyd, J. J.; Brothers, E.; Kudin, K. N.; Staroverov, V. N.; Kobayashi, R.; Normand, J.; Raghavachari, K.; Rendell, A.; Burant, J. C.; Iyengar, S. S.; Tomasi, J.; Cossi, M.; Rega, N.; Millam, J. M.; Klene, M.; Knox, J. E.; Cross, J. B.; Bakken, V.; Adamo, C.; Jaramillo, J.; Gomperts, R.; Stratmann, R. E.; Yazyev, O.; Austin, A. J.; Cammi, R.; Pomelli, C.; Ochterski, J. W.; Martin, R. L.; Morokuma, K.; Zakrzewski, V. G.; Voth, G. A.; Salvador, P.; Dannenberg, J. J.; Dapprich, S.; Daniels, A. D.; Farkas, Ö.; Foresman, J. B.; Ortiz, J. V.; Cioslowski, J.; Fox, D. J. Gaussian, , *Inc., Wallingford CT, 2009.*